We'am Sami

Department of Physics, College of Education, University of Al-Qadisiyah, Qadisiyah, IRAQ

Physical and Magnetic Properties of $Ni_{1-x}Cd_xFe_2O_4$ Ferrites Synthesized by Glycine-Nitrate Auto-Combustion Process

In this work, magnetic spinel $Ni_{1-x}Cd_xFe_2O_4$ ferrites (where x = 0, 0.4, and 0.6) were synthesized through glycine-nitrate auto-combustion process. Physical and magnetic properties that reported through XRD analysis, surface morphology, FTIR analysis, and magnetic measurement confirmed the formation of spinel structure for all ferrites with secondary phase of CdO with the crystallite size decreases from 32.09nm to 20.59nm with the increase of Cd^{2+} ion content for x = 0.4. FE-SEM images show that pure Ni-ferrite nanoparticles possess agglomeration. With increasing cadmium content at x=0.6, the morphology of the particles slightly changes. The agglomeration slightly enhance and spherical nanoferrites formation. FTIR spectra present the slight shift of the higher absorption band to low wavenumber for (x=0.4 and 0.6), which confirms the formation of $Ni_{1-x}Cd_xFe_2O_4$ spinel structure. Results show that, saturation magnetization decreased as the Cd content increases.

Keywords: Spinel ferrite; Glycine; Nanoparticles; Magnetic properties
Received: 15 February 2024; **Revised:** 02 May 2024; **Accepted:** 09 May 2024

1. Introduction

The preparation of the crystalline spinel ferrites in nano size plays a significant role in determining their physical properties at nano and sub-nano levels [1-3]. Ferrites are classified as ferromagnetic electro-ceramics that are consist of ferric oxide along with other metal with a general formula MFe_2O_4, where M is divalent metal ion such as Ni^{2+}, Cd^{2+} of the Ni-Cd ferrite [4,5]. The physical, chemical, and magnetic properties of ferrites in the nanosize regime are influenced by particle size [6,7]. The metal ions are distributed in two sub-lattices in spinel ferrites, namely the tetrahedral (A-site) and octahedral (B-site), based on the geometrical configuration of the oxygen nearest neighbors [8,9]. Nickel ferrite is one of the soft ferrite materials and due to ferrimagnetic properties and high electrochemical stability [1], it has several applications in technological fields such as photocatalytic degradation, biomedical efficiency, and cancer hyperthermia and information systems and data storage devices [10-13]. Nickel ferrite has a spinel ferrite with an inverse structure that is based on a face-centered cubic lattice of oxygen ions with an eight-unit unit cell, with all Ni ions occupy octahedral site and iron ions located in both tetrahedral and octahedral sites [14,15]. The various techniques to synthesis nickel ferrite were examined in a publication published in 2020. Co-precipitation, micro-emulsion method, solid-state [13], hydrothermal method, reactive sputtering, and sol-gel auto combustion method are the most commonly utilized methods [3,16]. When cadmium is added to nickel ferrite, a novel composite material with good magnetic properties is produced [17]. However, there hasn't been much research done on Ni-Cd ferrites nanoparticles thus far. Thus, in present work, we have reported synthesis of Ni-Cd ferrite nanoparticles using glycine-nitrate auto-combustion process.

2. Material and Methods

Nitrate salts of nickel ($Ni(NO_3)_2{\bullet}6H_2O$), cadmium ($Cd(NO_3)_2{\bullet}6H_2O$), and iron ($Fe(NO_3)_3{\bullet}9H_2O$) from HIMEDIA Co., India were used as raw materials. The following experimental steps were taken to synthesize $Ni_{1-x}Cd_xFe_2O_4$ ferrite samples, where x=0, 0.4 and 0.6, by glycine-nitrate auto-combustion process: (i) the required amount of nitrates was weighed separately with a molar ratio 1:2 for Ni-Cd:Fe, respectively and dissolved in a suitable quantity of de-ionized water, (ii) the solution was thoroughly mixed for 20 minutes by a magnetic stirrer at auto-combustion temperature 100°C, (iii) an amount of glycine was added to the nitrate solution as a fuel with G/N ratio of 0.33 without heat exchange. The self-sustaining combustion process was started in the system once the entire amount of water was vaporized, (iv) the product powder was washed via ethanol and distilled water for 4 times, dried at 80°C for 2 hours, and (vi) mortar was used to grind the resulting powder for 4 minutes to result in fine powder.

3. Results and Discussion

The as-synthesized ferrites were structurally characterized using Shimadzu X-ray diffractometer. The phase formation and structure analyses for all synthesized series samples are shown in Fig. (1). As compared with the standard pattern (00-054-0964) and (00-005-0674) of the Ni and Cd ferrites, respectively, the formation of phase cubic spinel structure is confirmed by prominent diffraction peaks (111), (220), (311), (222), (400), (422), (511), (440), (620), and (533).

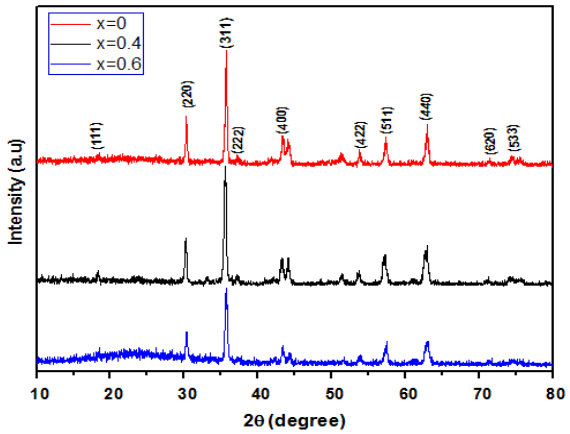

Fig. (1) XRD patterns of $Ni_{1-x}Cd_xFe_2O_4$ ferrite series samples

When Ni^{2+} ions are replaced by Cd^{2+} ions, there is a tiny shift to there is a tiny shift to high 2θ values. This suggests that indicates an decrease in lattice parameter, such shift indicates that this decrease in lattice parameter may be justified by the difference in ionic radius between Cd^{2+} (0.97Å), Ni^{2+} (0.69Å) ions and Fe^{3+} (0.49Å) [3,13] is the cause of the displacement. Furthermore, the small-sized nanoparticles in all samples were found to be responsible for the large bread width of the peaks in all patterns. Structure parameters such as crystallite size (*D*) and lattice constant (*a*) were calculated using the equations below from XRD line broadening of the highest peak (311) plane, as well as the distance between magnetic ions (hopping length) in A site (tetrahedral) and B site (octahedral) were calculated by using the complying relations (LA and LB) [14,15] and tabulated in table (1).

$$D = \frac{0.9\lambda}{\beta \cos\theta} \quad (1)$$

$$a = d\sqrt{(h^2 + k^2 + l^2)}\ \text{Å} \quad (2)$$

$$n\,\lambda = 2\,d\sin\theta \quad (3)$$

$$LA = \frac{a \times\sqrt{3}}{4},\ LB = \frac{a \times\sqrt{2}}{4} \quad (4)$$

In Debye-Scherrer's relation (Eq. 1), λ indicates the x-ray wavelength (1.542Å), θ is the Bragg's diffraction angle corresponding to the most intense reflection plane (311), and β is the full-width at half maximum (FWHM). Bragg's law (Eq. 3) was used to determine the inter planer spacing (*d*)

From table (1), it is clear that the crystallite size decreases from 32.09 to 20.59 nm with the increase of Cd^{2+} ion content for x=0.4 but this decrease is not continuous as the crystallite size will increase at x=0.6, which can be illustrated as the distance between the magnetic ions (hopping length), which increases as Cd content increases. This behavior of hopping length with x is analogous with behavior of '*a*' with x, and may be attributed to the difference in the ionic radii of the constituent ions [16] where an ionic radius of Ni^{2+} ions is smaller than the ionic radius of Cd^{2+} ions [3]. This is consistent with Bakale et al. for Ni-Cd ferrite, and Reyes-Rodríguez et al. and W. Sami et al. for other spinel ferrites [17,18]. Furthermore, based on the earlier research [19], the crystallite size is related to the value of pH. However, crystallite size does not decrease continuously with an increase in Cd ions, and is related to the pH value. When the pH value is too high, there is a lot of gas emitted during combustion process, leading to a decrease in crystallite size. Literature state that the lattice constant and crystallite size are directly related. Increasing in crystallite size lead to decrease or increase in the lattice constant [20]. In the present work, for the decrease in the crystallite size at x=0.4, the lattice constant has increased to 8.3612Å.

The surface morphology for spinel $Ni_{1-x}Cd_xFe_2O_4$ nanoparticles was recorded using a TESCAN Mira3 field-emission scanning electron microscope (FE-SEM). The FE-SEM images of all as-synthesized ferrites are depicted in Fig. (2).

FE-SEM images show that pure Ni-ferrite nanoparticles agglomerate due to their magnetic nature and the binding of initial particles held together by weak surface interactions such as the Van der Waals force. The holes and apertures in the photographs can also be attributed to the release of a massive volume of gas formed by the combustion's decomposition. Similar observations were seen in other ferrites [21]. However, with increasing Cd content to x=0.6, the morphology of the particles slightly changes. The agglomeration slightly enhance and spherical ferrite nanoparticles are formed. The impact of substitution Ni^{2+} by Cd^{2+} on the microstructure of Ni-ferrite can be explained as follows: Cd^{2+} substitution enhances grain growth of Ni-ferrite as a reaction center by increasing bulk diffusion due to aberration and activation of crystal lattice caused by substituted Cd^{2+}. Similar observations were seen in Ref. [13] for Ni-Cd ferrite and Ref. [22] for Ni-Zn ferrite.

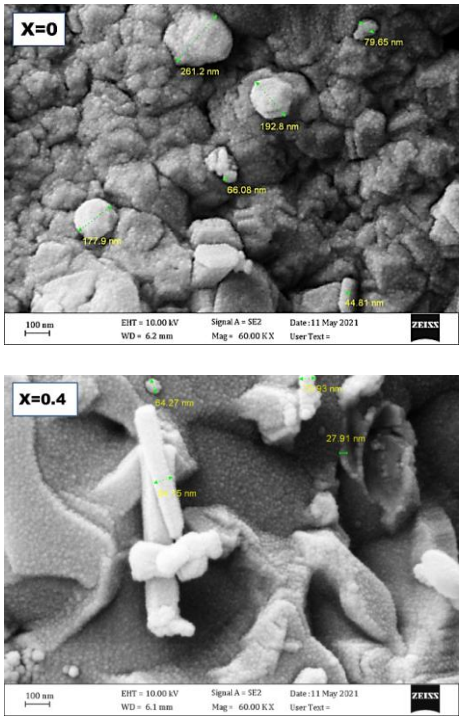

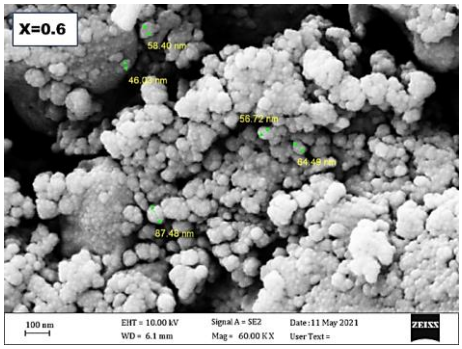

Fig. (2) FE-SEM images of the spinel $Ni_{1-x}Cd_x$ Fe_2O_4 ferrite series samples

To determine the chemical structure of the as-synthesis samples, the FTIR spectra were recorded using a Shimadzu 8400S FTIR spectrometer in the wavenumber range of 4000-450 cm^{-1}, as shown in Fig. (2).

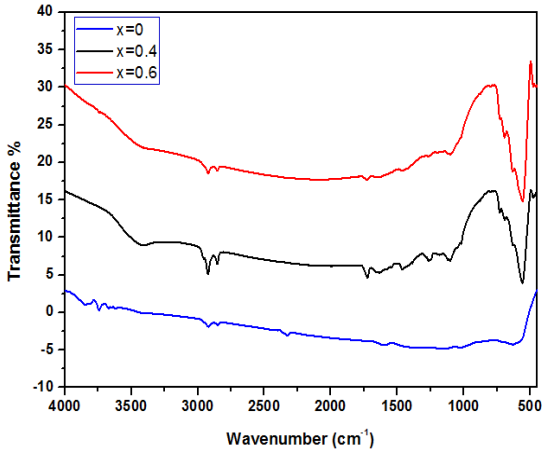

Fig. (3) FT-IR spectra of the spinel $Ni_{1-x}Cd_x$ Fe_2O_4 ferrite series samples

The spinel ferrite nanoparticles are known to have two FTIR-active bands, one is higher absorption band designated as υ_{Tet} and the other one is lower absorption band designated as υ_{Oct} in the range of 450-900 cm^{-1} [23]. In the present study, FT-IR spectra of all samples exhibit two intense peaks at 629 cm^{-1} (higher peak) and 459.70 cm^{-1} (lower peak) and correspond to the metal oxygen bonds. Higher and lower frequency bands are associated with oxygen-tetrahedral (Fe-O) and oxygen-octahedral (O-Fe-O) bending vibrations, respectively [14]. They are the characteristic peak of the spinel structure [24]. The significant Fe–O vibrational mode clearly showed that strong Cd doping occurred in $NiFe_2O_4$ spinel lattice. The hydroxyl group can be assigned to the wide band around 3400 cm^{-1}, while the in-plane and out-plane of O–H vibration can be assigned to the bands around 1630-1384 and 970-880 cm^{-1}, respectively. The remaining bands are most likely attributable to overtones or combinational frequencies. Similar variation was observed in Ref. [10]. The band positions (υ_{Tet}) and (υ_{Oct}) in the current ferrite system have been observed to change significantly as Ni^{2+} is replaced by Cd^{2+}. This could be related to the distribution of Cd^{2+} in the tetrahedral A-site, which replaces Fe^{3+} [13]. In the present series samples of $Ni_{1-x}Cd_xFe_2O_4$ ferrites the nickel divalent cations are stabilized in octahedral crystal field, while cadmium divalent cations are occupied tetrahedral sites due to the ability to form covalent connections involving sp3 hybrid orbitals. Higher and lower absorption band, as well as force constant for tetrahedral K_{Tet} and octahedral K_{Oct} of the series samples of $Ni_{1-x}Cd_xFe_2O_4$ ferrites are summarized in table (2). The force constant (k) was calculated using the following relation [25]:

$$k = 4\pi^2 \upsilon^2 c^2 \mu \quad (5)$$

where υ is the vibration frequency of the tetrahedral and octahedral sites, c is the light velocity, and μ is the reduced mass of the Fe^{3+} ion and the O^{2-} ions (2.065×10^{-23} g/mol)

Table (2) Tetrahedral and octahedral absorption band as well as force constants of the $Ni_{1-x}Cd_xFe_2O_4$ ferrite series samples

x	D (nm)	a (Å)	υ_{Tet} (cm^{-1})	υ_{Oct} (cm^{-1})	$K_{Tet}\times10^2$ N. m^{-1}	$K_{Oct}\times10^2$ N. m^{-1}
0	32.09	8.3321	629.00	-	2.87	-
0.4	20.59	8.3612	558.86	478.30	2.27	1.66
0.6	21.23	8.3303	476.71	459.70	1.65	1.53

Interestingly, the slight shift of the higher absorption band υ_{Tet} towards the lower wavenumbers is observed with an increase of Cd-substitution, which is attributed to decreased force constants and contraction of Fe^{3+}-O^{2-} bond lengths at both tetrahedral and octahedral sites, where force constants are directly related to the stretching and bending of chemical bonds [26]. These results are consistent with previously reported FTIR spectrum in Ref. [13].

The magnetic measurements are determined using a MDK vibrating sample magnetometer (VSM). Figure (4) shows the magnetic hysteresis loop for the mixed spinel $Ni_{1-x}Cd_xFe_2O_4$ ferrite at room temperature with applied external field of 15 kOe.

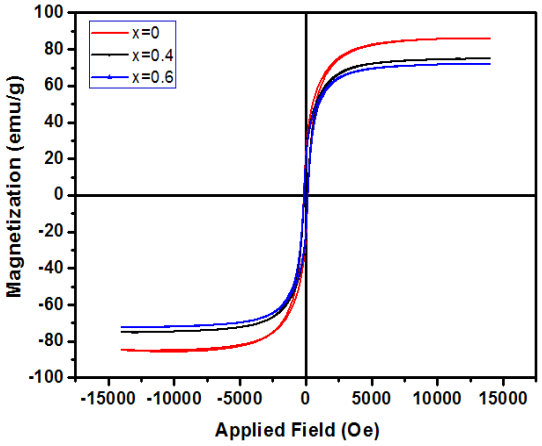

Fig. (4) Magnetization (emu/g) versus applied magnetic field (Oe) of $Ni_{1-x}Cd_xFe_2O_4$ ferrite at room temperature

As can be seen from both hysteresis curve and table (2), the Ni-Cd ferrites prepared in this work showed a S-shape hysteresis curve with high value of saturation magnetization and narrow loop that brought the low coercivity values. The saturation magnetization decreased as the Cd content is increased. In the present series of $Ni_{1-x}Cd_xFe_2O_4$ (where x=0, 0.4, and 0.6), magnetic nickel divalent cations are replaced by non-magnetic cadmium divalent cations and magnetic iron trivalent cations are replaced by non-magnetic cadmium divalent cations. As a result, the A-B interaction decreases in the system then the value of saturation magnetization decrease. Similar results were reported in Ref. [13].

Table (2) Magnetic measurements extracted from hysteresis loops of the spinel $Ni_{1-x}Cd_xFe_2O_4$ ferrite

Sample	x	Ms (emu/g)	Mr (emu/g)	Mr/Ms
$NiFe_2O_4$	0	86.04	29.15	0.338
$Ni_{0.6}Cd_{0.4}Fe_2O_4$	0.4	75.03	29.00	0.386
$Ni_{0.4}Cd_{0.6}Fe_2O_4$	0.6	72.31	28.00	0.387

4. Conclusion

In the present work, mixed spinel $Ni_{1-x}Cd_xFe_2O_4$ ferrite was synthesized using the glycine-nitrate auto-combustion process where x=0, 0.4, and 0.6. We found that the glycine-nitrate auto-combustion process has simplicity that is usually performed in solution media. Also, the lattice constant increases with increasing the Cd content at x=0.4 but this increase is not continuous as the lattice constant will be decrease at x=0.6. The $Ni_{1-x}Cd_xFe_2O_4$ ferrite showed soft ferrite with S-shape and pure nickel ferrite has higher saturation magnetization value but when nickel ions (Ni^{+2}) are replaced by cadmium ions (Cd^{+2}), a decrease in saturation magnetization has been exhibited.

References

[1] S. Sagadevan, Z.Z. Chowdhury and R.F. Rafique, "Preparation and Characterization of Nickel Ferrite Nanoparticles via Co-precipitation Method", *Mater. Res.*, 21 (2018) 1-5.

[2] O.A. Hammadi and N.E. Naji, "Fabrication and Characterization of Polycrystalline Nickel Cobaltite Nanostructures Prepared by Plasma Sputtering as Gas Sensor", *Phot. Sen.*, 8(1) (2018) 43-47.

[3] A. El-Mahdi and I. bin Selima, "Non-Equilibrium Plasma Assisted Combustion Kinetics", Iraqi J. Mater., 2(3) (2023) 97-106.

[4] S. Iraqui, S.S. Kashyap and Md.H. Rashid, "$NiFe_2O_4$ Nanoparticles: An Efficient and Reusable Catalyst for The Selective Oxidation of Benzyl Alcohol to Benzaldehyde Under Mild Conditions", *Nanoscale Adv.*, 2 (2020) 1-35.

[5] A.K. Nandanwar et al., "Effects of Ni^{2+}-Substitution on Structural, Magnetic and Electrical Properties of Cadmium Spinel Ferrite Nanoparticles via Chemical Route", *Integ. Ferroelect.*, 203 (2019) 12-18.

[6] J. Jacob and M. Abdul Khadar, "Investigation of Mixed Spinel Structure of Nanostructured Nickel Ferrite", *Conf. Ser.: J. Appl. Phys.*, 107 (2010) 1-10.

[7] A.J. Raheem and S.M. Raji, "Nickel Ferrite Nanostructures Prepared by DC Reactive Magnetron Sputtering", Iraqi J. Appl. Phys. Lett., 7(2) (2024) 7-10.

[8] A. Samavati and A.F. Ismail, "Antibacterial Properties of Copper-Substituted Cobalt Ferrite Nanoparticles Synthesized by Co-Precipitation Method", *Particuology*, 30 (2017) 1-6.

[9] J.O. Sattar, "Fabrication and Characterization of Nickel Cobaltite Nanostructures for Gas Sensing Applications", Iraqi J. Appl. Phys. Lett., 7(2) (2024) 15-18.

[10] S. Hirthna et al., "Synthesis and Characterization of $NiFe_2O_4$ Nanoparticles for the Enhancement of Direct Sunlight Photocatalytic Degradation of Methyl Orange", *J. Supercond. Novel Magnet.*, 31 (2018) 3315-3322.

[11] H.Q. Alijani et al., "Bimetallic Nickel-Ferrite Nanorod Particles: Greener Synthesis Using Rosemary and Its Biomedical Efficiency", *Artif. Cells Nanomed. Biotech.*, 48 (2020) 242-251.

[12] D. Saykova et al., "Synthesis and Characterization of Core–Shell Magnetic Nanoparticles $NiFe_2O_4$@Au", *metals*, 10 (2020) 1-13.

[13] C. Cherpin et al., "Study of The Solid-State Synthesis of Nickel Ferrite ($NiFe_2O_4$) by X-ray Diffraction (XRD), Scanning Electron Microscopy (SEM) and Raman Spectroscopy", *Materials*, 14 (2021) 1-9.

[14] M. De, A. Mukherjee and H.S. Tewari, "Characterization of Cadmium Substituted Nickel Ferrites Prepared Using Auto-Combustion Technique", *Process. Appl. Ceram.*, 9 (2015) 193-197.

[15] D. Guragain et al., "Effect of Terbium Ion Substitution in Inverse Spinel Nickel Ferrite: Structural and Magnetic Study", *Magnetochem.*, 6 (2020) 1-14.

[16] J. Haman, "New Geometrical Arrangement to Prepare Nickel Ferrite Nanostructures on Glass Substrates Using DC Reactive Magnetron Sputtering", Iraqi J. Sci. Ind. Res., 3(2) (2024) 42-46.

[17] K. Rafeekali and E.M. Muhammed, "Antibacterial Study of Cadmium Substituted Nickel Ferrite Nano Particles", *Int. J. Eng. Res. General Sci.*, 3 (2015) 321-324.

[18] S.P. Jadhav et al., "Effect of Cadmium Substitution on Structural and Magnetic Properties of Nano Sized Nickel Ferrite", *Chinese J. Chem. Phys.*, 23 (2010) 459-464.

[19] W.A. Farooq et al., "Structural, Optical and Electrical Properties of $Cu_{0.6}Co_xZn_{0.4-x}Fe_2O_4$

(x=0.0, 0.1, 0.2, 0.3, 0.4) Soft Ferrites", *Molecules*, 26 (2021) 1-10.
[20] P. Bakale et al., "Synthesis, Structural and Mechanical Properties of $Ni_{1-x}Cd_xFe_2O_4$ Ferrites (x=0.1, 0.2, 0.3, and 0.4)", *Int. J. Adv. Sci. Eng.*, 6 (2019) 1285-1290.
[21] B.H. Devmunde, P.S. Bhalerao and M.B. Solunke, "Structural Morphological and Infrared Properties of Cd^{2+} Substitutes Nickel Ferrite Particles", *J. Phys.: Conf. Ser.*, 1644 (2020) 1-8.
[22] P.Y. Reyes-Rodríguez et al., "Structural and Magnetic Properties of Mg-Zn Ferrites ($Mg_{1-x}Zn_xFe_2O_4$) Prepared by Sol-Gel Method", *J. Mag. Mag. Mater.*, 427 (2017) 268-271.
[23] W. Sami and Z.S. Sadeq, "Synthesis, Characterizations, and Magnetic Properties of Mixed Spinel $Mg_{1-x}Zn_xFe_2O_4$ Ferrites", *Iraqi J. Sci.*, 63 (2022) 997-1003.
[24] Q. Lin et al., "Magnetic and Mössbauer Spectroscopy Studies of Zinc-Substituted Cobalt Ferrites Prepared by the Sol-Gel Method", *Materials*, 11 (2018) 1-12.
[25] L.R. Nivedita et al., "Correlation Between Crystal Structure, Surface/Interface Microstructure, and Electrical Properties of Nanocrystalline Niobium Thin Films", *J. Nanomater.*, 10 (2020) 1-23.
[26] P.A. Udhaya, M. Meena and M.A.J. Queen, "Green Synthesis of $MgFe_2O_4$ Nanoparticles Using Albumen as Fuel and Their Physico-Chemical Properties", *Int. J. Sci. Res. Phys. Appl. Sci.*, 7 (2019) 71-74.
[27] S.B. Khan, S. Irfan and S.-L. Lee, "Influence of Zn^{+2} Doping on Ni-Based Nanoferrites ($Ni_{1-x}Zn_xFe_2O_4$)", *Nanomater.*, 9 (2019) 1-17.
[28] M.A. Ansari et al., "Synthesis and Characterization of Antibacterial Activity of Spinel Chromium-Substituted Copper Ferrite Nanoparticles for Biomedical Application", *J. Inorg. Organomet. Polym. Mater.*, 28 (2018) 2316-2327.
[29] W. Sami, and Z.S. Sadeq, "Synthesis and Study of Calcination Effect of Zinc Ferrite on the Structure and Morphology of Nanoparticles", *J. Phys. Conf. Ser.*, 1999 (2021) 1-10.
[30] C. Kumari et al., "Structural and Optical Properties of Nanosized Co Substituted Ni Ferrites by Coprecipitation Method", *Phase Trans. A Multinational J.*, 93 (2020) 207-216.
[31] A. Abbasi, "Structural and Spectroscopic Studies of Solvated Metal Ions", PhD thesis, Stockholm University (2005), 8.

Table (1) Crystallite size and lattice constant, and hopping length for A site (Tetrahedral) and B site (Octahedral) of the $Ni_{1-x}Cd_xFe_2O_4$ ferrite series samples

As-synthesized powder samples	x	2θ (deg)	FWHM (deg)	d (Å)	Lattice Constant a (Å)	Crystallite Size D(nm)	hopping length	
							L_A	L_B
$NiFe_2O_4$	0	35.7113	0.25590	2.51223	8.3321	32.09	3.6077	2.9458
$Ni_{0.6}Cd_{0.4}Fe_2O_4$	0.4	35.5829	0.38450	2.52100	8.3612	20.59	3.6205	2.9561
$Ni_{0.4}Cd_{0..6}Fe_2O_4$	0.6	35.7191	0.37390	2.51170	8.3303	21.23	3.6071	2.9452

